Time-Domain Response Envelope for Structural Dynamic Systems

Jay-Chung Chen,* Marc Trubert,* and John A. Garba†
Jet Propulsion Laboratory, California Institute of Technology, Pasadena, California

A transient envelope solution method is developed for payload structural systems. This method requires that the external forcing functions are decomposed into a quasistatic and dynamic parts. The amplitude of the peak envelope and the corresponding varying frequencies for the generalized forcing functions are required for obtaining the response envelopes. The proposed method is applied to a spacecraft structural system and the results are in good agreement with the exact solution.

Nomenclature

$a(t)$ = transient envelope solution
A,B = defined in Eq. (29)
$A(N)$ = mean value of the dynamic part of the generalized force
$f_0(t)$ = quasistatic component of the external forcing function
$f_1(t)$ = slowly varying coefficient associated with $\cos\Omega t$ of the external forcing function
$F(t)$ = external forcing function
$[\ I\ ]$ = identity matrix
$[k_l]$ = launch vehicle stiffness matrix
$[k_{12}],[k_{21}]$ = stiffness coupling between payload and launch vehicle
$[k_{22}]$ = cantilevered payload stiffness matrix
$[m_{rr}]$ = rigid body mass, Eq. (6)
$[m_l]$ = launch vehicle mass matrix
$[m_2]$ = payload mass matrix
n = number of data points in the original discretization of the generalized forces
N_S = number of data points in each subset
N_T = number of subsets of the new discretization for envelope solution
$\{u\}$ = payload modal responses
$\{u_0\}$ = quasistatic component of the modal responses
$\{u_1\}$ = transient component of the modal responses
$\{x_e\}$ = payload elastic motion
$\{x_I\}$ = launch vehicle/payload interface DOF connecting payload to launch vehicle, a subset of the launch vehicle DOF $\{x_l\}$
$\{x_l\}$ = launch vehicle degrees of freedom (DOF)
$\{x_2\}$ = payload DOF
Δt = time interval associated with the original discretization
Δt = time interval for each subset, Eq. (36)
α = stiffness coefficient of Eq. (16)
$\theta(t)$ = polar coordinate defined in Eq. (18)
$[\ \rho\ ]$ = modal damping matrix for payload
σ = damping coefficient of Eq. (16)
$\sigma(N)$ = standard deviation of the data in Nth subset
$[\phi]$ = payload normal mode matrix
$[\phi_R]$ = payload rigid-body transformation matrix defined as the payload displacement due to unit displacement of the launch vehicle/payload interface DOF
$\phi(t)$ = slowly varying phase angle
$[\omega^2]$ = payload eigenvalue matrix
$\Omega(t)$ = slowly varying frequency of the external forcing function

Submitted April 29, 1983; presented as Paper 83-0818 at the AIAA/ASME/ASCE/AHS Structures, Structural Dynamics and Materials Conference, Lake Tahoe, Nev., May 2-4, 1983; revision submitted Aug. 10, 1984.

*Member of Technical Staff. Member AIAA.
†Supervisor, Structures and Dynamics Technology Group. Member AIAA.

Introduction

IN loads analysis for aerospace payloads, two different methods are generally used to obtain the loads for design purposes. One is the full-scale system transient analysis in which a complete launch vehicle/payload composite model is subjected to the external forcing functions representing the dynamic environments. The time-domain solutions are then obtained for the response or load histories for which the pertinent values for the design process can be extracted.[1,2] The method provides the most accurate predictions for responses and loads; however, it is organizationally tedious and time consuming as well as computationally costly due to the large amount of integation steps. Also, its results are highly sensitive to the model changes. This means that a new iteration is required whenever a design change occurs. Some approximation methods have been developed to overcome the shortcomings of the transient solution method.[3-5] Another method is the shock spectra method in which an upper bound of responses and loads are obtained. This method is organizationally simple and inexpensive. Also, the results are not as sensitive to the design changes.[6] The disadvantages are that the results tend to be conservative and the designer is not able to predict time phasing for the computed maximum values. A survey of the various loads analysis methods and their comparisons can be found in Ref. 7.

The Natures of the Dynamic Environments

For aerospace payloads, usually the design dynamic environments come from the liftoff transients, staging events, aerodynamic loadings, etc. Therefore, the forcing functions which are simulating a specific dynamic environment in the mathematical model are highly transient in nature. Figure 1 shows the flight-measured low-frequency environments during the power phase of the mission for the Voyager spacecraft whose launch vehicle consists of a three-stage Titan rocket and a Centaur upper stage. Figure 2 shows the Space Shuttle (STS-5) low-frequency cargo bay ascent environments. Both flight measurements show that the transient signals consist of a steady-state signal (dc) superimposed by a periodic signal with varying amplitude and frequency.

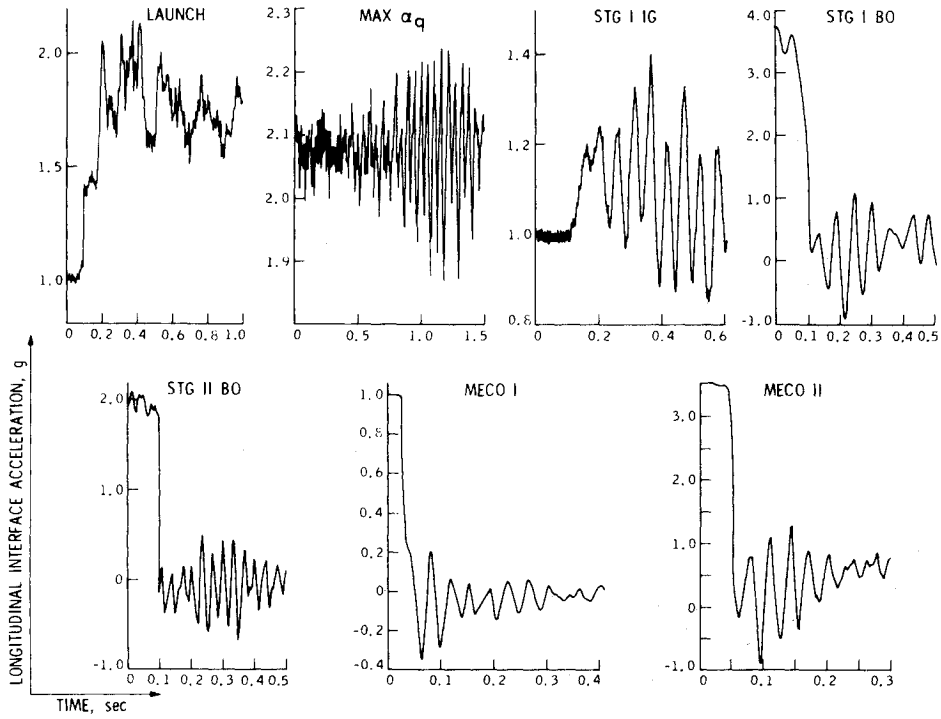

Fig. 1 Flight-measured Voyager Spacecraft acceleration at the interface.

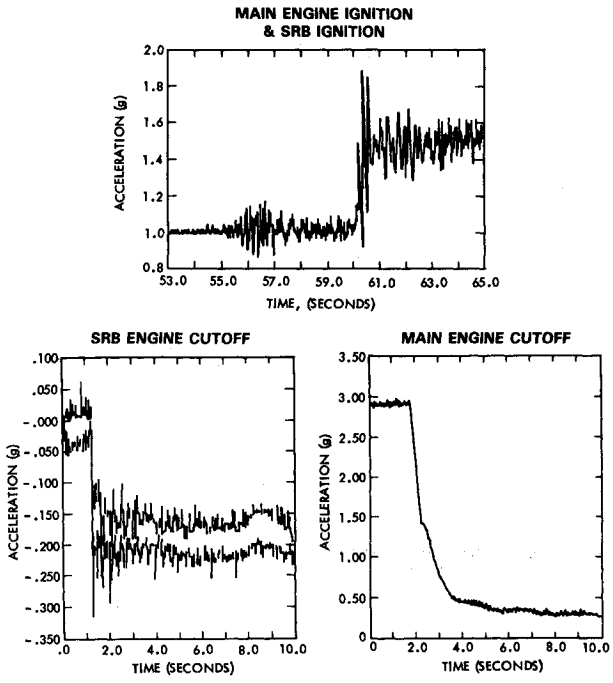

Fig. 2 Space Shuttle (STS-5) cargo bay ascent environment.

Without loss of generality, these types of transient forcing functions can be decomposed into

$$F(t) = f_0(t) + f_1(t)\cos\Omega t \tag{1}$$

where Ω is a time-varying function. $f_0(t)$, $f_1(t)$, and Ω are varying slowly with respect to time, but the product $f_1(t)\cos\Omega t$ is a rapid time-varying function. Figure 3 shows graphically how a typical transient forcing function can be decomposed as indicated by Eq. (1). It is obvious that the coefficient function $f_1(t)$ is the envelope of the peaks of the variable periodic signal.

Since the responses of the payload structural system are governed by a linear second-order differential equation, one may expect that the responses will also be transient similar in nature as the forcing functions. When the response values are to be used in the structural design process, the maximum values should be selected instead of specific values at any particular time; i.e., it is the envelope of the peaks that is of interest instead of the complete transient solution. The objective of the present study is to calculate the envelope of the transient peaks of the response from the envelope of the forcing function directly without having to perform a full-scale transient solution. Because the envelope is varying slowly with respect to time, fewer integration steps are required such that the computational cost can be greatly reduced.

Governing Equations

The detailed derivation for the finite element formulation of payload structural dynamic system has been developed in previous studies.[3,4] Only the governing equations will be examined briefly:

$$\begin{bmatrix} m_1 & 0 \\ 0 & m_2 \end{bmatrix} \begin{Bmatrix} \ddot{x}_1 \\ \ddot{x}_1 \end{Bmatrix} + \left(\begin{bmatrix} k_1 & 0 \\ 0 & 0 \end{bmatrix} + \begin{bmatrix} k_{11} & k_{21} \\ k_{12} & k_{22} \end{bmatrix} \right) \begin{Bmatrix} x_1 \\ x_2 \end{Bmatrix} = \begin{Bmatrix} F(t) \\ 0 \end{Bmatrix} \tag{2}$$

Although damping is not included in Eq. (2), it will be incorporated later in the form of modal damping. Also, for simplicity, it will be assumed herein that the payload is supported in a statically determinate manner such that

$$[k_{11}] = [\phi_R]^T [k_{22}] [\phi_R]$$
$$[k_{21}] = -[\phi_R][k_{22}] = [k_{12}]^T \tag{3}$$

Next, the motion of the payload will be decomposed into two parts, namely, the rigid-body motion and the elastic motion:

$$\{x_2\} = [\phi_R]\{x_1\} + \{x_e\} \tag{4}$$

The first term on the right-hand side of Eq. (4) is the rigid-body motion. The second term, $\{x_e\}$, is the elastic motion or relative motion with reference to the interface. It should be noted that only the elastic motion $\{x_e\}$ will generate internal loads in the structure. Using Eqs. (3) and (4), Eq. (2) can be transformed into the following form:

$$\begin{bmatrix} m_1+m_{rr} & \phi_R^T m_2 \\ m_2\phi_R & m_2 \end{bmatrix} \begin{Bmatrix} \ddot{x}_1 \\ \ddot{x}_2 \end{Bmatrix} + \begin{bmatrix} k_1 & 0 \\ 0 & k_{22} \end{bmatrix} \times \begin{Bmatrix} x_1 \\ x_2 \end{Bmatrix} = \begin{Bmatrix} F(t) \\ 0 \end{Bmatrix} \tag{5}$$

where

$$[m_{rr}] = [\phi_R]^T [m_2] [\phi_R] \tag{6}$$

is denoted as rigid-body mass.

From Eq. (5), the payload elastic degrees of freedom (DOF) are governed by

$$[m_2]\{\ddot{x}_e\} + [k_{22}]\{x_e\} = -[m_2][\phi_R]\{\ddot{x}_1\} = -[m_2][\phi_R]\{\ddot{x}_1\} \tag{7}$$

Equation (7) indicates that the payload elastic response can be calculated once the interface acceleration $\{\ddot{x}_1\}$ has been determined.

In the present study, Eq. (7) will be treated as the governing equation for the payload structural system. The left-hand side of Eq. (7) represents the analytical model constructed by the analysts and the right-hand side represents the prescribed external forcing function. Equation (7) will be rewritten as

$$[m]\{\ddot{x}\} + [k]\{x\} = -[m_2][\phi_R]\{\ddot{x}_1\} \tag{8}$$

Let

$$\{x\} = [\phi]\{u(t)\} \tag{9}$$

where $[\phi]$ is the normal mode matrix such that

$$[\phi]^T [m] [\phi] = [\ I\ ]$$

$$[\phi]^T [k] [\phi] = [\ \omega^2\ ] \tag{10}$$

Then, the governing equation (9) can be transformed into generalized coordinates as

$$\{\ddot{u}\} + [\ 2\rho\omega\ ]\{\dot{u}\} + [\ \omega^2\ ]\{u\} = \{F(t)\} \tag{11}$$

where

$$\{F(t)\} = -[\phi]^T [m_2][\phi_R]\{\ddot{x}_1\} = \text{generalized force} \tag{12}$$

Since the payload/launch vehicle interface acceleration $\{\ddot{x}_1\}$ possesses precisely the characteristics shown in Figs. 1 and 2, the elements in the generalized force vector $\{F(t)\}$ can be expanded similar to Eq. (1). Then the solution of Eq. (11) can be expressed approximately as

$$\{u(t)\} \cong \{u_0(t)\} + \{u_1(t)\} \tag{13}$$

where

$$[\ \omega^2\ ]\{u_0(t)\} = \{f_0(t)\} \tag{14}$$

$$\{\ddot{u}_1\} + [\ 2\rho\omega\ ]\{\dot{u}_1\} + [\ \omega^2\ ]\{u_1\} = \{f_1(t)\cos\Omega t\} \tag{15}$$

$u_0(t)$ is basically an approximate static solution which is only valid if the quasistatic part $f_0(t)$ of the forcing function signal is, indeed, very slowly varying with respect to time.

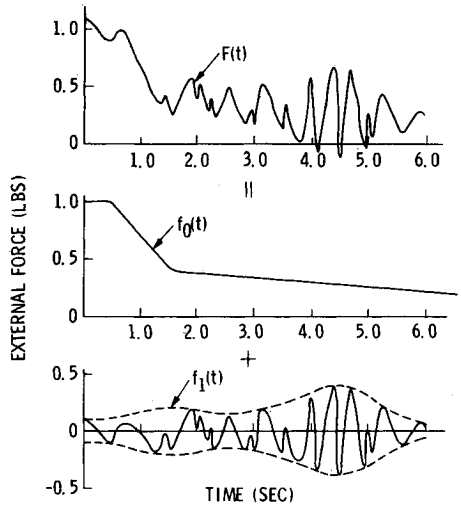

Fig. 3 Forcing function decomposition.

Since Eqs. (14) and (15) are completely uncoupled, they will be written in scalar form from now on. The amplitude envelope of the forcing function in Eq. (15), $f_1(t)$, is slowly varying with respect to time as the flight data indicate. Instead of the transient solution, the envelope of $u_1(t)$ will be sought.

Method of Slowly Varying Parameters

This method is also known as the method of Bogoliuboff and Mitropolski,[8] and has been used in solving nonlinear vibration problems. For a given differential equation

$$\frac{d^2x}{dt^2} + \sigma\frac{dx}{dt} + \alpha x = F(t)\cos\Omega t \tag{16}$$

the solution will be assumed to be

$$x(t) = a(t)\cos[\Omega t - \phi(t)] \tag{17}$$

where $F(t)$, $a(t)$, and $\phi(t)$ are slowly varying with respect to time. Let,

then $$\theta(t) = \Omega t - \phi(t) \tag{18}$$

$$\frac{dx}{dt} = -a\Omega\sin\theta + a\frac{d\phi}{dt}\sin\theta + \frac{da}{dt}\cos\theta \tag{19}$$

Since $a(t)$ and $\phi(t)$ are slowly varying, da/dt and $d\phi/dt$ are small; therefore, it is assumed[9] that

$$\frac{da}{dt}\cos\theta + a\frac{d\phi}{dt}\sin\theta = 0 \tag{20}$$

Then

$$\frac{dx}{dt} = -a\Omega\sin\theta \tag{21}$$

and

$$\frac{d^2x}{dt^2} = -a\Omega^2\cos\theta - \frac{da}{dt}\Omega\sin\theta + a\Omega\frac{d\phi}{dt}\cos\theta \tag{22}$$

Upon substitution into Eq. (16), one obtains

$$-a\Omega^2\cos\theta - \frac{da}{dt}\Omega\sin\theta + a\Omega\frac{d\phi}{dt}\cos\theta + f(a,\theta) = F(t)\cos\Omega t \tag{23}$$

where

$$f(a,\theta)\theta=\alpha\frac{dx}{dt}+\alpha x=-\alpha a\Omega\sin\theta+\alpha a\cos\theta \tag{24}$$

Multiplying Eq. (21) by $\Omega\sin\theta$ and Eq. (23) by $\cos\theta$, and adding the results, will give

$$a\Omega\frac{d\phi}{dt}-a\Omega^2\cos^2\theta+f(a,\theta)\cos\theta=F(t)\cos(\theta+\phi)\cos\theta \tag{25}$$

If $a(t)$, $\phi(t)$ and $F(t)$ are slowly varying functions, one may postulate that they remain constant over one cycle of $\theta(t)$. Then an averaging procedure will be performed as

$$\frac{1}{2\pi}\int_0^{2\pi}[\text{Eq. (25)}]\,d\theta=0$$

which gives

$$2\Omega\bar{a}\frac{d\bar{\phi}}{dt}+(\alpha-\Omega^2)\bar{a}=F\cos\bar{\phi} \tag{26}$$

Similarly, multiplying Eq. (21) by $\Omega\cos\theta$ and Eq. (23) by $\sin\theta$, subtracting the results, and taking the average, gives

$$2\Omega\frac{d\bar{a}}{dt}+\alpha\Omega\bar{a}=F\sin\bar{\phi} \tag{27}$$

where the bar denotes an average value over one cycle.

Next, another transformation will be performed by Eq. (26) $\times\cos\bar{\phi}+$ Eq. (27) $\times\sin\bar{\phi}$ and Eq. (27) $\times\cos\bar{\phi}-$ Eq. (26) $\times\sin\bar{\phi}$. The resulting equations are

$$\frac{dA}{dt}+\frac{\sigma}{2}A-\frac{(\alpha-\Omega^2)}{2\Omega}B=0$$

$$\frac{dB}{dt}+\frac{\sigma}{2}B+\frac{(\alpha-\Omega^2)}{2\Omega}A=\frac{F(t)}{2\Omega} \tag{28}$$

where

$$A(t)=\bar{a}\cos\bar{\phi}\quad\text{and}\quad B(t)=\bar{a}\sin\bar{\phi} \tag{29}$$

Note that in Eq. (28) the bar has been neglected.

The envelope of the solution, $a(t)$, can be obtained as

$$a(t)=[A^2(t)+B^2(t)]^{1/2} \tag{30}$$

Now, applying the method of slowly varying parameters to the solution of Eq. (15), let

$$u_l(t)=A(t)\cos\Omega t+B(t)\sin\Omega t \tag{31}$$

the amplitude $A(t)$ and $B(t)$ can be obtained by solving the following equations:

$$\frac{dA}{dt}+\frac{\sigma}{2}A-\frac{(\alpha-\Omega^2)}{2\Omega}B=0$$

$$\frac{dB}{dt}+\frac{\sigma}{2}B+\frac{(\alpha-\Omega^2)}{2\Omega}A=\frac{F(t)}{2\Omega} \tag{32}$$

and the envelope of u_l can be obtained from Eq. (30). From Eqs. (13-15) the upper and lower bounds of the generalized coordinate $u(t)$ can be expressed as

$$u(t)\,|_{\text{upper}}=(1/\omega^2)f_0(t)+a(t) \tag{33}$$

$$u(t)\,|_{\text{lower}}=(1/\omega^2)f_0(t)-a(t) \tag{34}$$

These upper and lower bounds are much more meaningful than the individual peaks in the response comparison since no phase-matching problem exists. Also, due to the slowly varying nature, a much larger time interval can be used in calculating the numerical solutions for Eq. (32). This makes the procedures more cost-effective.

Example of Galileo Spacecraft Loads Analysis

Galileo is an interplanetary spacecraft whose mission is to conduct scientific exploration of the planet Jupiter. It is to be launched by the Shuttle/Centaur in 1986. Figure 4 shows the spacecraft in launch configuration with its major component indicated. The total weight of the spacecraft is approximately 5300 lb. A finite element model using the NASTRAN code has been constructed for loads analysis with a total of 10,000 elastic DOF and 300 mass DOF. The first 70 modes of the modal analysis were retained covering the natural frequencies from 12.78 to 82.88 Hz.

The loads analysis for Galileo was done by a complex combination of generalized shock spectra analysis, transient analysis, and mass acceleration curve, the details of which are not the subject of this paper. Only an example of the application of the envelope method to a selected portion of the Galileo spacecraft is reported here.

The forcing function at the right-hand side of Eq. (8) is represented by the interface acceleration $\{\ddot{x}_I\}$ obtained at JPL by coupled launch vehicle/spacecraft transient analysis. These are six time-history functions representing three translational and three rotational accelerations at the interface. Figures 5 and 6 show two typical translational interface acceleration time histories and their corresponding shock spectra plots. The interface acceleration time history contains $n=2500$ discrete data points for an event duration of 10 s. Therefore, the transient solution for Eq. (11) needs 2500 integration steps to obtain the complete time history for a modal response. Since 70 spacecraft modes are considered for the loads analysis, this integration procedure is repeated 70 times to construct the time history for the modal response vector $\{u(t)\}$. For computing the physical responses, matrix multiplication as expressed by Eq. (9) must be performed 2500 times. These are some of the main reasons that a transient response analysis is costly.

The envelopes of the forcing function are established at the generalized force level as shown in Eq. (12). Figure 7 describes the procedure used in the present study where $g(t)$ is the actual time history subtracted by the quasistatic part. The original discretization of the time history consists of n data points with the corresponding time interval Δt. The envelope

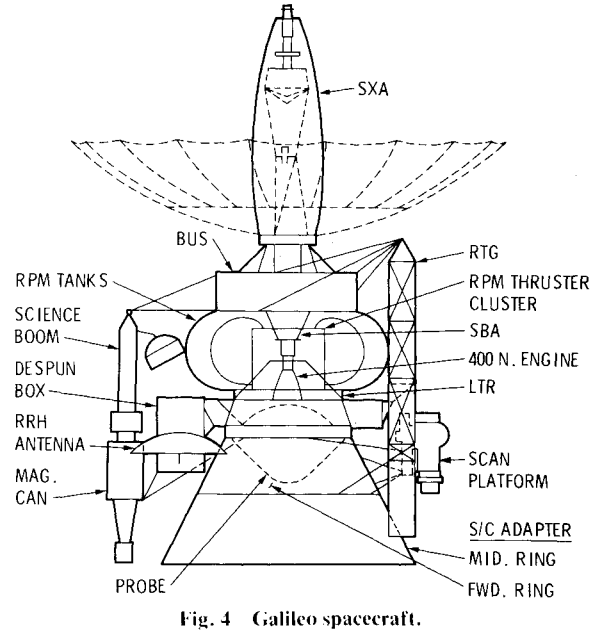

Fig. 4 Galileo spacecraft.

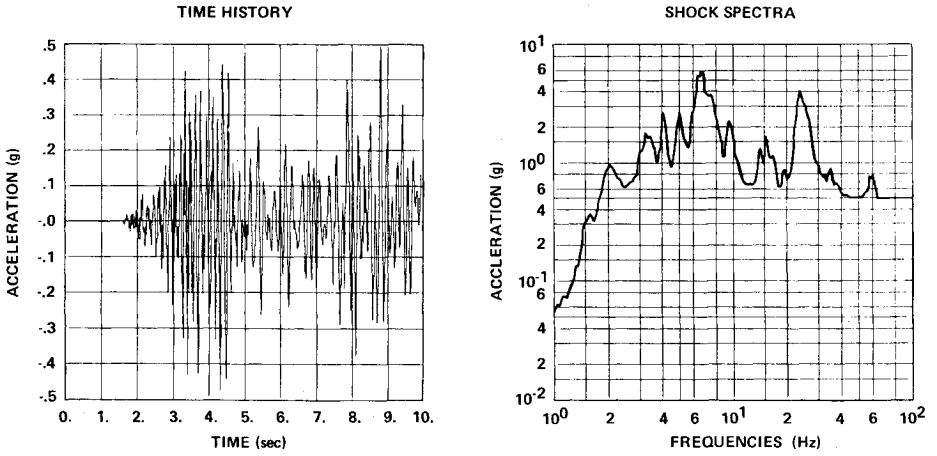

Fig. 5 Shuttle/payload interface acceleration, lateral.

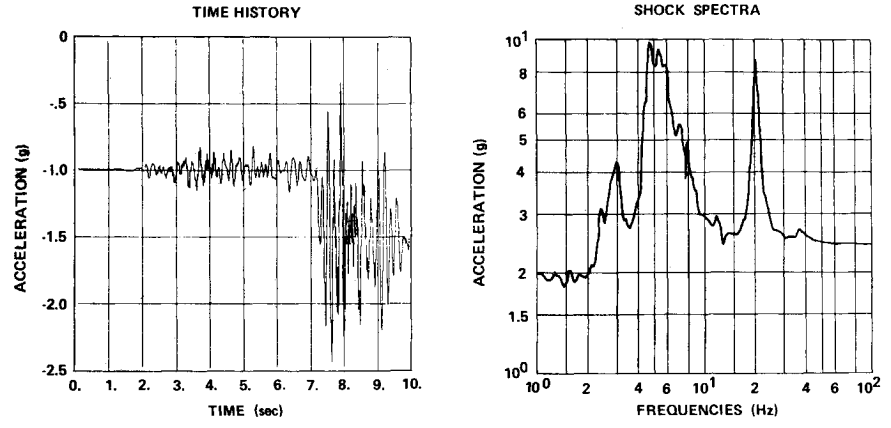

Fig. 6 Shuttle/payload interface acceleration, axial.

will be discretized into a total of N_T subsets, each containing N_S original data points. Therefore,

$$N_S = n/N_T \tag{35}$$

and the time interval for the new discretization will be Δt, such that

$$\Delta t = N_S \times \Delta t \tag{36}$$

The original time history of the generalized force can be written as

$$F(j) = F(t)\,|_{t=j\Delta t} \tag{37}$$

where $j=0,1,2,\ldots,n$.

The decomposed forcing function as shown in Eq. (1) will be defined in the new discretization

$$f_0(N) = f_0(t)\,|_{t=N\cdot\Delta t}$$

$$f_1(N) = f_1(t)\,|_{t=N\cdot\Delta t} \tag{38}$$

where $N=0,1,2,\ldots,N_T$.

The slowly varying quasistatic part of the decomposed forcing function $f_0(t)$ can be obtained as follows:

$$f_0(0) = f(N=0) = \frac{1}{(N_S/2)} \sum_{j=0}^{\frac{1}{2}N_S} F(j), \qquad N=0$$

$$f_0(N) = \frac{1}{N_S} \sum_{j=-\frac{1}{2}N_S}^{\frac{1}{2}N_S} F(N\cdot N_S + j) \qquad 0<N<N_T$$

$$f_0(N_T) = \frac{1}{N_S/2} \sum_{j=-\frac{1}{2}N_S}^{0} F(N_T N_S + j), \qquad N=N_T \tag{39}$$

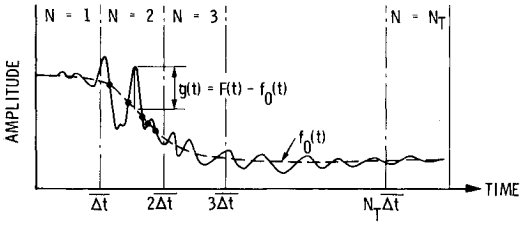

Fig. 7 Discretization for envelope solution.

Next, the mean value of the dynamic part of the generalized force for each subset will be defined as

$$A(N) = \frac{1}{N_S+1} \sum_{j=N\cdot N_S}^{(N+1)N_S} [F(j) - f_0(N)] \tag{40}$$

The mean square of the subset will be

$$\sigma^2 = \frac{1}{N_S+1} \sum_{j=N\cdot N_S}^{(N+1)N_S} [F(j) - f_0(j) - A(N)]^2 \tag{41}$$

Finally, the amplitude of the envelope $f_1(N)$ will be written as

$$f_1(N) = A(N) + 3.0\sigma(N) \tag{42}$$

Within each subset, the number of zero crossings of the dynamic part of the generalized force decomposition will be counted and the frequency Ω of the subset is defined as

$$\Omega(N) = \left.\frac{\text{No. of zero crossings}}{2}\right|_{N\text{th subset}} \times 2\pi(\text{rad/s}) \tag{43}$$

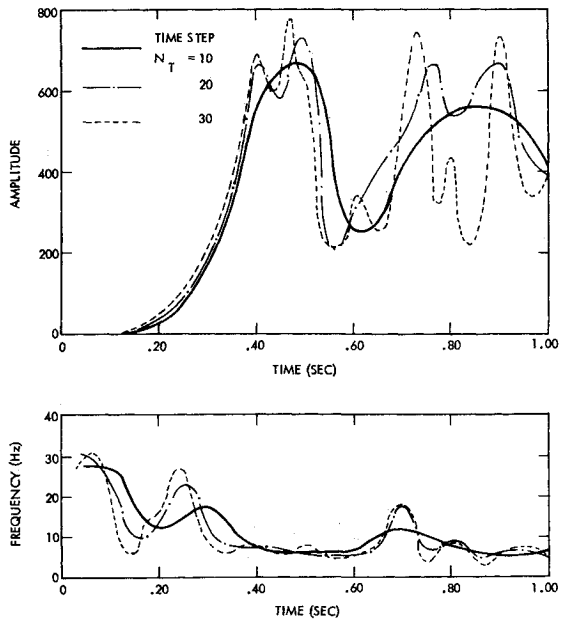

Fig. 8 Mode 1 generalized forcing function envelope.

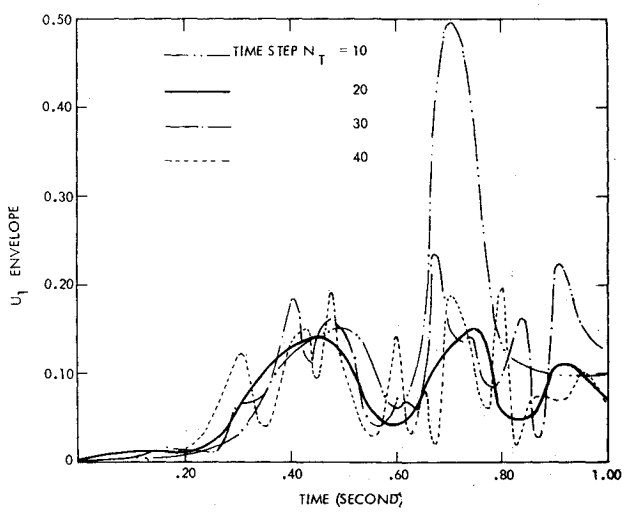

Fig. 9 Envelopes of first modal response.

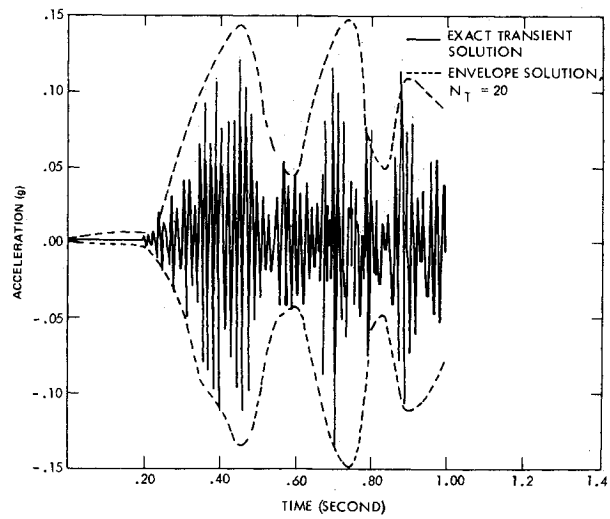

Fig. 10 Envelope and transient solution comparison for first modal response.

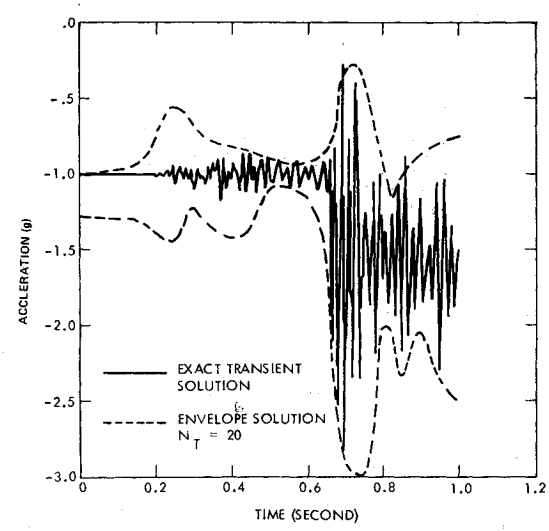

Fig. 11 Envelope and transient solution comparison for high-gain antenna.

It should be noted that in the subsequent calculation for obtaining the solutions of Eq. (32), the time interval and total numbe of time steps will be Δt as expressed in Eq. (36) and N_I, respectively, instead of Δt and n.

Based on the described procedue, the envelope of the generalized force and its corresponding time-varying frequencies for the first mode are shown in Fig. 8 for various numbers of subsets or time steps, N_I. For $N_I = 10$ and 20, the amplitudes of the envelopes are generally in agreement. For $N_I = 30$, the amplitude changes more rapidly than the previous cases. This is due to averaging over a fewer number of data points and changes with shorter intervals. It should be noted that the constraint of "slowly varying" parameters must be observed. Therefore, smaller size subsets N_S may not be desirable for this method. The time-varying envelope frequencies obtained for different N_I show general agreement with one another.

With decomposed generalized forces, the envelopes of the modal responses for the 70 modes are calculated. Figure 9 shows that of the first mode for various values of N_I. As expected, envelopes obtained for $N_I = 10$ and 20 are reasonably slow varying and those obtained for $N_I = 30$ and 40 show rapid changes. Except around $t = 0.7$ s, the envelopes from $N_I = 10$ and 20 are in good agreement. The disagreement can be traced back to the frequency $\Omega(t = 0.7) = 12.5$ Hz for $N_I = 10$. Since modal frequency of the first mode is 12.78 Hz, the high amplitude for the case is due to the resonance.

Figure 10 shows the comparsion of the modal response envelope with the exact transient solution which is obtained by the Duhamel's integral method. The agreement is excellent. It should be noted that although 10 s of forcing function were available as indicated in Figs. 5 and 6, only 1 s of data immediately before and after the liftoff were used. This period represents the most severe dynamic environment as shown in Figs. 8-11. The integration steps for the 1-s duration is 250 times for the transient solution and 20 times for the envelope solution. Also, the integration routine for the envelope solution is much simpler since the governing equation is only first order as compared to the second-order differential equation for the transient solution.

Figure 11 shows the response comparison for the high-gain antenna. The responses are calculated by multiplying the modal acceleration vector by the modal matrix as shown in Eq. (9). The multiplication operation must be performed 250 and 20 times for the transient and envelope solutions, respectively. Again, the agreement between the two is very

Table 1 Comparison of maximum acceleration (g)

Node	DOF	Transient solution	Envelope solution			
			$N_T=10$	$N_T=20$	$N_T=30$	$N_T=40$
(1180)	1	1.95	10.2	5.14	7.12	7.41
High-gain antenna	2	13.8	14.0	10.7	26.7	11.40
c.g.	3	2.88	2.55	3.02	2.87	3.03
(1188)	1	6.70	20.2	7.71	16.3	13.8
High-gain antenna	2	45.0	27.0	28.0	53.3	61.1
Tip	3	2.89	2.56	3.04	2.88	3.05
(3160)	1	0.90	2.33	2.43	1.86	2.97
Oxygen tank	2	2.28	4.45	4.74	8.32	10.8
	3	3.76	4.39	4.16	5.41	5.14
(3260)	1	0.84	3.03	3.13	3.13	4.02
Fuel tank	2	1.89	5.00	6.02	8.98	11.2
	3	3.37	3.29	4.02	4.96	4.95
(3360)	1	0.94	1.67	0.97	1.12	2.10
Oxygen tank	2	2.08	4.63	5.71	8.90	12.14
	3	3.63	2.43	2.56	2.53	2.76
(3460)	1	0.92	2.43	3.04	3.35	4.0
Fuel tank	2	2.30	4.70	5.55	8.47	11.1
	3	2.95	2.16	2.25	2.33	2.40
(6100)	1	1.16	0.31	0.39	0.38	0.36
Scan platform	2	1.89	0.72	1.99	2.62	3.00
	3	3.53	2.54	2.34	2.34	3.57
(7050)	1	1.32	0.28	0.38	0.41	0.48
RTG + X	2	2.40	0.38	0.87	0.60	0.69
	3	8.31	3.20	3.25	4.23	6.40
(7550)	1	0.91	1.06	1.06	1.12	1.02
RTG − X	2	3.03	2.18	3.41	3.27	3.18
	3	6.06	6.62	19.91	14.2	10.1
(8130)	1	0.89	0.75	1.72	1.56	1.78
Probe	2	3.97	2.96	12.1	13.6	13.5
	3	2.95	2.52	2.71	2.55	2.70

good. It should be noted that the lower bound envelope solution does not begin at zero due to the average mean value assigned to the first subset. Table 1 shows the comparisons of various maximum responses obtained by the two methods. The reason that a few of the maximum responses from the transient analysis exceed those of the envelope solution is attributed to the rather simple way for the construction of envelopes of the generalized forces. It is possible that peaks in the generalized forces exceed the envelopes which are 3σ values of the values in the subset. A more elaborate algorithm to generate the amplitude of the envelope would most likely result in a better envelope solution.

Although Figs. 10 and 11 indicate that a good envelope indeed can be obtained by using $N_T=20$, the detailed comparison in Table 1 shows that actually using $N_T=30$ seems to provide a better response estimate. At the present time, the choice of N_T will have to be dependent on each individual's judgment by examining the responses carefully.

Concluding Remarks

One of the shortcomings of design load analysis is the fact that the entire process for complex structures is often tedious, complicated, expensive, and time consuming. Therefore, the results are seldom utilized by the designers in a timely fashion and iteratively with the design modifications.[10] In the present investigation a method is developed by which the response envelopes, the upper and lower bounds, can be calculated directly from the envelopes of the forcing functions. These envelopes can be obtained not only in a very cost-effective manner, but also can provide maximum response value for the design process. The method retains the advantages from both the transient loads prediction, i.e., accuracy and the shock spectra loads estimation, i.e., simplicity. The method is demonstrated by the example of Galileo spacecraft loads analysis.

It should be emphasized here that the present method is developed for the purpose of estimating loads for the design process in which the structural system will be modified for various reasons. The prerequisites of the method are 1) a payload/launch vehicle coupled transient analysis for the establishment of loaded interface acceleration $\{\ddot{X}_I\}$, and 2) the generalized forces $\{F(t)\}$ in Eq. (12). In other words, the proposed method cannot completely replace the system transient analysis in the loads analysis effort, at least, not at present.

In summary, the present investigation provided an approach by which the accurate loads estimation can be used in the detailed structural design process in a cost-effective and timely manner.

Acknowledgments

The research presented here was carried out under the auspices of the Applied Mechanics Division of the Jet Propulsion Laboratory, California Institute of Technology, under NASA Contract NAS7-100. The effort was supported by Samuel L. Venneri, Materials and Structures Division, Office of Aeronautics and Space Technology, National Aeronautics and Space Administration.

References

[1] Wada, B.K., "Design of Space Payloads for Transient Environments," ASME AMD Vol. 36, *Survival of Mechanical Systems in Transient Environments*, Dec. 1979, pp. 61-89.

[2] Ryan, R.S., Bullick, T., Holland, W.B., Kross, D.A., and Kiefling, L.A., "System Analysis Approach to Deriving Design Criteria (Loads) for Space Shuttle and Its Payloads," Vol. I and II, NASA TP, 1950, Dec. 1981.

[3] Chen, J.C., Wada, B.K., and Garba, J.A., "Launch Vehicle Payload Interface Response," *Journal of Spacecraft and Rockets*, Vol. 15, Jan.-Feb. 1978, pp. 7-11.

[4]Chen, J.C., Garba, J.A., and Wada, B.K., "Estimation of Payload Loads Using Rigid-Body Interface Acceleration," *Journal of Spacecraft and Rockets*, Vol. 16, March-April 1979, pp. 74-80.

[5]Chen, J.C., Zagzebski, K.P., and Garba, J.A., "Recovered Transient Load Analysis for Payload Structural Systems," *Journal of Spacecraft and Rockets*, Vol. 18, July-Aug. 1981, p. 374-379.

[6]Trubert, M. and Salama, M., "A Generalized Shock Spectra Method for Spacecraft Loads Analysis," *AIAA Journal*, Vol. 18, Aug. 1980, pp. 988-994.

[7]Chen, J.C., Garba, J.A., Salama, M., and Trubert, M., "A Survey of Load Methodologies for Shuttle Orbiter Payloads," Jet Propulsion Laboratory, California Institute of Technology, Pasadena, Calif., JPL Pub. 80-37, June 15, 1980.

[8]Bogoliuboff, N.N. and Mitropolski, *Asymotic Methods in the Theory of Nonlinear Oscillation*, Hindustan Publishing Co., 1961.

[9]Nayfeh, A.H. and Mook, D.T., *Nonlinear Oscillations*, John Wiley & Sons, New York, 1979.

[10]Amos, A.K. and Goetz, R.C., "Research Needs in Aerospace Structural Dynamics," *Proceedings of the AIAA/ASME/ASCE/AHS 20th Structures, Structural Dynamics and Materials Conference*, St. Louis, Mo., April 1979, pp. 390-394.